

# MULTI-OBJECTIVE SURROGATE BASED OPTIMIZATION OF GAS CYCLONES USING SUPPORT VECTOR MACHINES AND CFD SIMULATIONS

Khairy Elsayed<sup>1,2</sup>, Chris Lacor<sup>1</sup>

<sup>1</sup> Vrije Universiteit Brussel, Department of Mechanical Engineering, Research Group Fluid Mechanics and Thermodynamics, Pleinlaan 2, 1050 Brussels, Belgium,  
{kelsayed, chris.lacor}@vub.ac.be

<sup>2</sup> Mechanical Power Engineering Department, Faculty of Engineering at El-Mattaria, Helwan University, Masaken El-Helmia P.O., Cairo 11718, Egypt, kelsayed75@gmail.com

**Key words:** Cyclone Separator, Surrogate Models, Support Vector Machines, Multi-Objective Optimization.

**Abstract.** In order to accurately predict the complex non-linear relationships between the cyclone performance parameters (The Euler and Stokes numbers) and the four significant geometrical dimensions (the inlet section height and width, the vortex finder diameter and the cyclone total height), the support vector machines approach has been used. Two support vector regression surrogates (SVR) have been trained and tested by CFD data sets. The result demonstrates that SVR can offer an alternative and powerful approach to model the performance parameters. The SVR model parameters have been optimized to obtain the most accurate results from the cross validation steps. SVR (with optimized parameters) can offer an alternative and powerful approach to model the performance parameters better than Kriging. SVR surrogates have been employed to study the effect of the four geometrical parameters on the cyclone performance. The genetic algorithms optimization technique has been applied to obtain a new geometrical ratio for minimum Euler number and for minimum Euler and Stokes numbers. New cyclones over-perform the standard Stairmand design performance. A Pareto optimal solutions have been obtained and a new correlation between the Euler and Stokes numbers are fitted. CFD simulations for the Stairmand design and the new design for minimum Euler numbers are performed using the Reynolds stress turbulence model. The analysis of the CFD results reveal the changes in the flow field pattern which cause the better performance presented by the new design.

## 1 Introduction

Cyclone separators are widely used in gas-solid separation for aerosol sampling and industrial applications [79] where both the gravity and centrifugal force are used to separate

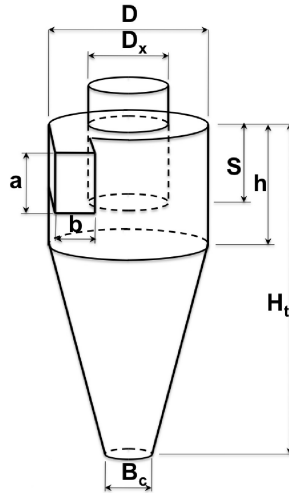


Figure 1: 3D view of cyclone geometry. In this study,  $h/D = 1.5$ ,  $S/D = 0.5$ ,  $B_c/D = 0.375$ .

solids from a mixture of solids and fluids. Cyclones have the following advantages. Simplicity in construction, contain no moving parts, relatively maintenance free, can handle high pressure and temperature mixtures and corrosive gases, relative economy in power consumption. Due to these advantages, cyclone separators have become one of the most important particle removal devices in both engineering and process operation [79] such as, cement industry, oil and gas, coal fired boiler, workshops and vacuum cleaners.

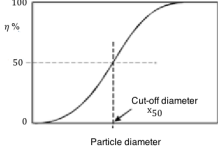
### 1.1 Cyclone geometry

The cyclone geometry is described by seven geometrical parameters, viz. the inlet height  $a$ , and width  $b$ , the vortex finder diameter  $D_x$  and length  $S$ , the cylinder height  $h$ , the cyclone total height  $H_t$  and cone-tip diameter  $B_c$  as shown in Fig. 1. It has been approved in previous studies by the authors that only four geometrical parameters significantly affect the cyclone flow pattern and performance [20–23, 25, 26, 28, 30]. The four significant factors are the inlet section height  $a$  and width  $b$ , the vortex finder diameter  $D_x$  and the cyclone total height  $H_t$ .

### 1.2 Cyclone performance

Besides the separation efficiency (or alternatively, the cut-off diameter for low mass particle loading), pressure drop is another major index for cyclone performance evaluation. Therefore, it is necessary to obtain an accurate model to determine the complex relationship between the performance parameters and the cyclone characteristics. Table 1 presents more details about the two performance parameters.

Table 1: The definition of the cyclone performance parameters

The Euler number $Eu$	The Stokes number $Stk_{50}$
<p>The Euler number is the dimensionless pressure drop <math>\Delta P</math>. <math>\Delta P = (\text{the area- and time-averaged static pressure at the inlet section}) - (\text{the area- and time-averaged static pressure at the gas exit section})</math>.</p> <p><math>Eu = \frac{\text{The pressure drop between the inlet and the gas exit}}{\text{The average kinetic energy at the inlet}}</math></p> <p><math>Eu = \frac{\Delta P}{\frac{1}{2}\rho V_{in}^2}</math> where <math>\rho</math> is the gas density and <math>V_{in}</math> is the average inlet velocity. <math>Eu</math> is not affected by operating conditions in the high Reynolds number range (<math>Re &gt; 5 \times 10^4</math>, <math>Re = \frac{\rho V_{in} D}{\mu}</math>) [20, 45].</p>	<p><math>Stk_{50}</math> is the dimensionless cut-off diameter <math>x_{50}</math>. <math>x_{50}</math> is the particle diameter that produces 50% collection efficiency. <math>Stk_{50} = \rho_p x_{50}^2 V_{in} / (18\mu D) = \frac{\tau_p}{\tau_f}</math> [17]. It is the ratio between the particle relaxation time (the time constant in the exponential decay of the particle velocity due to drag) <math>\tau_p = \rho_p x_{50}^2 / (18\mu)</math> and the gas flow integral time scale <math>\tau_f = D / V_{in}</math> where <math>\rho_p</math> is the particle density and <math>\mu</math> is the gas viscosity.</p> 

### 1.3 Literature review

To estimate the cyclone performance parameters there are five approaches:

1. Experimental investigations (e.g., Xiang et al. [74])
2. Theoretical and semi-empirical models (e.g., Stairmand [70])
3. Statistical models (e.g., Ramachandran et al. [62])
4. Computational fluid dynamics (CFD) (e.g., Chuah et al. [12], De Souza et al. [14], Elsayed and Lacor [20, 21, 23, 26, 28], Kaya and Karagoz [51])
5. Artificial intelligence techniques (e.g., Elsayed and Lacor [22, 25], Zhao and Su [80])

Table 2 presents a summary of these five approaches with a sample of the available studies in the literature.

The afore-mentioned prediction models (PR, KG and ANN) (cf. Table 2) have numerous drawbacks, which include locally optimal solutions, low generalization, over-fitting, and poor stability [54]. The support vector machine (SVM) surrogate can offer a better alternative to these models. In the field of performance evaluation for cyclone separators, unfortunately, SVM does not receive a great deal of attention on its algorithmic advantages. There is only one study using the support vector regression (SVR) on cyclone separator performed by Zhao [79]. Zhao [79] approved the potential of SVR to model the effect of cyclone geometry on the pressure drop (based on experimental dataset collected from different sources) but he did not go further to use the fitted SVR to study the effect of each parameter on the performance or for optimization. Moreover, he used the traditional approach to find suitable values for SVR parameters.

### 1.4 Target of this study

This study aims to:

- Apply the SVR surrogate to model the variation of the two cyclone performance parameters with the change in the most significant geometrical parameters based on CFD based data set.

- Introduce a computationally cheap framework for SVR parameter optimization using a Python code.
- Compare the accuracy of the fitted SVRs models with the KG models.
- Study the effect of each significant geometrical parameter on the cyclone performance using the SVR models.
- Optimize the cyclone performance for minimum Euler number as well as for best performance using multi-objective optimization technique.

## 2 Least Squares - Support Vector Regression (LS-SVR)

The least squares support vector regression (LS-SVR) was introduced by Suykens et al. [71] as a reformulation to the standard SVR. LS-SVR simplified the standard SVR model to a great extent by applying linear least squares criteria to the loss function instead of a traditional quadratic programming method [71, 73]. As excellent examples of the nonlinear dynamic system, least squares support vector regression (LS-SVR) based on the structured risk minimization principle has been successfully applied to many fields of function approximation and pattern recognition because of its high accuracy and generalization capabilities [6]. Compared with artificial neural networks, LS-SVR seeks to minimize an upper bound of the generalization error instead of the empirical error, and can provide more reliable and better generalization performance under the same training conditions [66].

In the LS-SVR model, the training dataset of  $l$  points is assumed to be  $x_k, y_k$  ( $k = 1, 2, \dots, l$ ), in which  $x_k \in R^n$  is the input vector and  $y_k \in R$  is the corresponding target vector. The regression problem can be transformed into the following optimization problem [54, 63]:

$$\underset{\omega, b, e_k}{\text{minimize}} \Psi(\omega, e) = \frac{1}{2} \omega^T \omega + \frac{C}{2} \sum_{k=1}^l e_k^2 \quad (1)$$

$$\text{subject to } y_k = \omega^T \phi(x_k) + b + e_k, \quad (k = 1, 2, \dots, l) \quad (2)$$

Where  $e_k$  is the error between the predicted value and the true value of the system,  $C > 0$  is the regularization parameter applied to minimize estimation error and control function smoothness,  $\phi(\cdot)$  denotes the nonlinear mapping from input spaces to feature space,  $\omega$  is an adjustable weight vector, and  $b$  is the bias (scalar threshold). Equation 2 is the constraint. In order to solve the optimization problem, the Lagrange function can be presented by the following equation:

$$L(\omega, b, e, \alpha) = \frac{1}{2} \omega^T \omega + \frac{C}{2} \sum_{k=1}^l e_k^2 - \sum_{k=1}^l \alpha_k \{ \omega^T \phi(x_k) + b + e_k - y_k \} \quad (3)$$

Table 2: Summary of the different approach used to estimate the cyclone performance

Approach	Comments
Experimental investigations	Different measurements techniques have been used to measure the cyclone performance parameters. At present Laser Doppler anemometry (LDA) [e.g. 48, 68] and particle image velocimetry (PIV) [e.g. 60, 75, 77] are frequently employed to study experimentally the flow structure in the cyclones. The experimental approach is very costly due to need to construct the cyclone as well as the expensive measuring equipment.
Theoretical and semi-empirical models	Theoretical or semi-empirical models were successively developed by many researchers, e.g., Shepherd and Lapple [64], Alexander [1], First [35], Stairmand [69], Barth [5], Avci and Karagoz [3], Zhao [78], Karagoz and Avci [49] and Chen and Shi [10]. These models were derived from physical descriptions and mathematical equations were based on a very detailed understanding of gas flow pattern and energy dissipation mechanisms in the cyclone. In addition, different assumptions and simplified conditions were used in these models, leading to either enormous error between the measured data and predicted results by these models or the conflict of these models when they were used to evaluate different types of cyclone [79].
Statistical models	The representative researches included the models proposed by Casal and Martinez-Benet [9], Dirgo [19] and Ramachandran et al. [62] to estimate the pressure drop. These models were developed through statistical regression analysis based on large data set for different cyclone configurations. Zhao [79] stated that although the statistical models are more convenient to predict the cyclone performance, it is rather difficult in this approach to determine the optimal correlation function for fitting experimental data.
Computational fluid dynamics (CFD)	Recently, the computational fluid dynamics (CFD) technique has presented a new way to model the cyclone performance. Several researchers successfully applied CFD calculation to predict and to evaluate the effects of different geometrical and operational parameters on the performance of gas cyclones. CFD is able to provide not only the performance parameters but also the detailed information of the flow field inside the cyclone. The main drawback of using CFD results is that it is computationally expensive to solve the Navier-Stokes equations using RANS such as Elsayed and Lacor [22, 26], Gimbin et al. [38, 39], Griffiths and Boysan [40], Hoekstra et al. [43], Hoffmann et al. [44], Qian and Zhang [61] or LES such as Derksen [16], Derksen et al. [18], Elsayed and Lacor [23, 28], Slack et al. [67]. Moreover, three levels of grid density is needed to achieve a grid independent results.
Surrogate models	<p>The application of surrogate models is much cheaper than the other techniques such as experimental or CFD especially if the target is to optimize the performance parameters. The widely used surrogate models in predicting the cyclone performance parameters are:</p> <p><b>Polynomial regression models (PR):</b> The simplest form is the second order polynomial regression. This kind of surrogate is suitable to mimic the input-output relationship of maximum quadratic relationships e.g. Elsayed and Lacor [20].</p> <p><b>Kriging (KG):</b> Kriging surrogate models recently used by the authors to model the effect of cyclone separator geometry on its performance, e.g., Elsayed and Lacor [27, 31], Elsayed et al. [34].</p> <p><b>Artificial neural networks (ANNs):</b> With the interdisciplinary development of modern computational technologies, artificial neural networks (ANNs), as typical artificial intelligence (AI) models and algorithms, have become an attractive approach for modeling highly complicated and nonlinear system without understanding the nature of phenomenon [79]. Radial basis function artificial neural networks (RBFNN) has been successfully used to mimic the cyclone performance in many studies such as Elsayed and Lacor [22, 27, 29], Zhao and Su [80]. However, ANN has been applied in many studies, ANN has some limitations.</p> <ul style="list-style-type: none"> <li>- Unlike other models, ANN does not provide information about the relative importance of the various parameters [63].</li> <li>- The knowledge acquired during the training of the model is stored in an implicit manner and hence it is very difficult to come up with reasonable interpretation of the overall structure of the network [52].</li> <li>- In addition, ANN has some inherent drawbacks such as slow convergence speed, less generalizing performance, arriving at local minimum and over-fitting problems.</li> </ul> <p><b>Support vector machines (SVM):</b> SVM is a supervised learning theory from the field of machine learning applicable to both nonlinear classification called SVMC or SVC and regression called SVMR or SVR. Rooted in the statistical learning theory developed by Vapnik [72], SVM quickly gained attention from many research areas due to a number of theoretical and computational merits and marked the beginning of a new era in the learning from examples paradigm [79]. In recent years, SVM is fast becoming a powerful tool of scientific research and technological development. It has been successfully applied to many engineering fields [11].</p>

Where  $\alpha_k (k = 1, 2, \dots, l)$  are the Lagrange multipliers. Accordingly, the Karush-Kuhn-Tucker (KKT) conditions are used for optimality by differentiating  $L$  in Eq. (3) with the  $\omega, b, e_k$ , and  $\alpha_k$ , which is shown as follows [54]:

$$\begin{cases} \frac{\partial L}{\partial \omega} = 0 \rightarrow \omega = \sum_{k=1}^l \alpha_k \phi(x_k) \\ \frac{\partial L}{\partial b} = 0 \rightarrow \sum_{k=1}^l \alpha_k = 0 \\ \frac{\partial L}{\partial e_k} = 0 \rightarrow \alpha_k = C e_k \\ \frac{\partial L}{\partial \alpha_k} = 0 \rightarrow \omega^T \phi(x_k) + b + e_k - y_k = 0 \end{cases} \quad (4)$$

Elimination of the  $x$  and  $e_k$  from Eq. (4) results in the following set of linear equations:

$$\begin{bmatrix} 0 & I^T \\ I & \Phi + C^{-1}I \end{bmatrix} \begin{bmatrix} b \\ \alpha \end{bmatrix} = \begin{bmatrix} 0 \\ Y \end{bmatrix} \quad (5)$$

where  $I$  is the unit matrix,  $\Phi = \phi(x_k)^T \phi(x) = K(x_k, x)$ ,  $Y = [y_1, y_2, \dots, y_l]^T$ . The resulting LS-SVR model for function estimation is obtained as:

$$\hat{y} = f(x) = \sum_{k=1}^l \alpha_k K(x_k, x) + b \quad (6)$$

In Eq. (6),  $K(x_k, x)$  is the kernel function which satisfies Mercers condition corresponding to a dot product in some feature spaces [57]. Four common Mercer kernel functions are widely used [54]:

**Linear kernel:**  $K(x_k, x) = x_k^T x$

**Polynomial kernel:**  $K(x_k, x) = (x_k^T x / \sigma^2 + \gamma)^d$

**RBF kernel:**  $K(x_k, x) = \exp(-\gamma \|x_k - x\|^2)$

**Sigmoid kernel:**  $K(x_k, x) = \tanh(\gamma x_k^T x + r)$

where  $d, \gamma$ , and  $\sigma$  are constants.

Because RBF kernels map samples into high dimensional space in a nonlinear fashion and have fewer parameters to set, and because this method handles the nonlinear relationship well and has an excellent overall performance, it is by far the most popular option for kernel function types [71]. This study consequently adopted an RBF kernel function, shown in Eq. (7) in order to contribute to the LS-SVR model's achieving optimal solution.

$$K(x_k, x) = \exp(-\gamma \|x_k - x\|^2) \quad (7)$$

Generally, LS-SVR solves linear equations and will lead to important reductions in calculation complexity. Compared with SVR, *LS-SVR is characterized by faster training speed, higher stability and better control strategy* [54, 63].

## 2.1 LS-SVR parameter optimization

*The LS-SVR performance heavily depends on the choice of several hyperparameters, which are necessary to define the optimization problem and the final LS-SVR model.*

To design an LS-SVR, one must choose a kernel function, set hyperparameters such as the kernel parameters, and determine a regularization parameter  $C$ . The hyperparameters that should be optimized include the regularization parameter  $C$  and the kernel function parameters such as  $\gamma$  for the radial basis function (RBF) kernel. Thus, selecting appropriate model parameters has a crucial impact on prediction accuracy. Unfortunately, there is no exact method to obtain the optimal set of LS-SVR hyperparameters; consequently, a search algorithm must be applied to obtain the parameters.

For the nonlinear LS-SVR, its generalization performance depends on the proper setting of parameters  $C$  and kernel parameters  $\gamma$ . Inappropriate hyperparameters combinations in LS-SVR lead to over-fitting or under-fitting. One procedure to obtain the LS-SVR parameters follows the trial and error approach to minimize some generalized error measures such as the mean squared error [4]. This procedure is time-consuming, tedious and unable, in many cases, to converge at the global optimum. Zhao [79] applied the two-step search technique to dynamically seek the optimal values for the LS-SVR parameters. The two steps are: First perform a coarse search to identify a better region in search field according to contour lines of MSE. Then perform a fine search over that region. The disadvantage of the multi-step search technique is that it will be more prone to be trapped in local optimum point especially if a limited number of points are used.

In this study, we propose an alternative approach. The proposed approach employs the simulated annealing optimization technique to heuristically seek the optimal values for the LS-SVR parameters that minimize the difference between the predicted and the true values.

Simulated annealing (SA) is an optimization technique that proposed by Kirkpatrick et al. [53]. SA attempts to find the global minimum of a cost function that may possess several local minimum. SA is able to deal with cost functions with quite arbitrary degrees of nonlinearities, discontinuities and stochasticity and can process quite arbitrary boundary conditions and constraints imposed on them [2]. The method works by imitating the physical process whereby a heated solid is slowly cooled. When eventually its structure is frozen, which happens at a minimum energy configuration. The slow cooling gives atoms more chances of finding configurations with lower internal energy than the initial ones [2].

From the initial state with fitness value  $E_1$ , the system can be perturbed stochastically leading to a new state with fitness value  $E_2$ . The newly generated state is accepted or rejected based on the following relation [76]:

$$P_A = \begin{cases} 1, & \text{if } E_2 < E_1 \\ \exp[-(E_2 - E_1)/T_i], & \text{otherwise} \end{cases} \quad (8)$$

Where parameter  $T_i$  is called analogous or synthetic temperature at the  $i$ th step, which

controls the cooling down or *annealing* dictated by user specified cooling schedule.

$$T_i = T_{i-1} - \Delta T, \quad i = 1, 2 \dots, N. \quad (9)$$

For  $T_0$  as starting value of temperature, and  $N$  number of total annealing steps:  $\Delta T = T_0/N$ . A large initial value of temperature allows more frequent up-hill moves enabling system to escape local minimum while the down-hill moves dominate like steepest descent for lower values of temperature near the end.

The simulated annealing (SA) is used in this study to optimize the parameters of SVR:  $C$  and kernel parameter  $\gamma$  of RBF-kernel function. In the training and testing process of LS-SVR, the objective is to minimize the errors between the actual and predicted values of the testing samples. Therefore, the objective (fitness) function of SA is the mean squared error from the cross validation.

In the parameters optimization process,  $K$ -fold cross validation is employed to avoid the over-fitting and to calculate the fitness function. The original sample is randomly partitioned into  $K$  subsamples. In these subsamples, a single subsample is used as the validation data for testing the model while the other  $K-1$  subsamples are used as training data. The cross validation process is then repeatedly performed  $K$  times, with each of the  $K$  subsamples selected exactly once as the validation data. The cross validation error is estimated as the average mean squared error (MSE) on test subsamples, as shown in Eq. (10). Commonly, 5-fold and 10-fold cross validation is the most widely used method. In this study, the 5-fold cross validations are employed to estimate the MSE.

$$\text{MSE} = \frac{1}{K} \sum_{j=1}^K \left( \sum_{i=1}^{Nt_j} (\hat{y}_i - y_i)^2 \right) \quad (10)$$

where  $K$  is the number of folds (5 in this study),  $Nt_j$  is the number of testing points in fold  $j$ ,  $y_i$  represents the actual values, and  $\hat{y}_i$  represents the predicted values.

Figure 2 presents a flow chart for the complete optimization framework. The main steps are explained as follows:

**Selection of the design variables :** In this study, the four significant design variables are selected  $a, b, D_x$  and  $H_t$ . This is based on several previous studies performed by the authors [20–23, 25, 26, 28].

**Design of experiment (DoE) :** The Statgraphics XVI has been used to create the sampling plan. The Box-Behnken design create 33 test cases. The minimum, center and maximum values of the four significant factors.

**Preparing the training CFD data set :** In this (most time consuming) process, three steps are performed. (1) Use the Gambit grid generator to create the cyclone geometry and create hexahedral meshes using gambit journal files. (2) The CFD



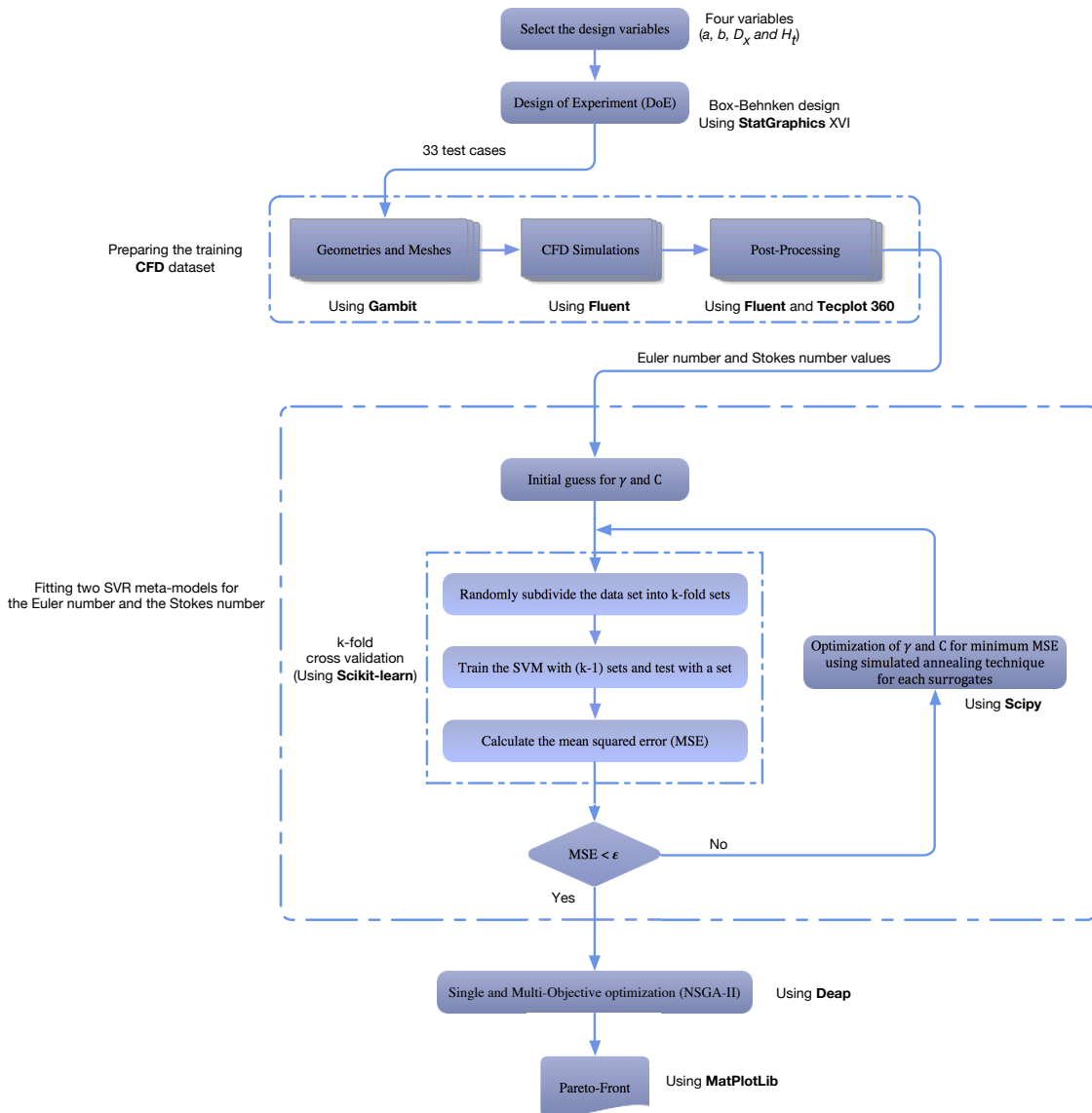


Figure 2: Flow chart for the complete optimization framework

simulations are performed using the Ansys Fluent 6.3.26. The simulations are automated by Fluent journal files. (3) The post-processing to estimate the pressure drop using the surface integral panel and consequently the Euler number. The discrete phase modeling has been used to inject particle with different diameter from the inlet. After constructing the grade collection efficiency curves. Tecplot is used to precisely estimate the cut-off diameter and consequently the Stokes number.

**Fitting the two SVR models :** This is the parameter optimization step. We start with initial guess for the two parameters  $\gamma$  and  $C$ . The simulated annealing (SA) from `Scipy` is used for optimization. The fitness function is the mean squared error MSE from the cross validation. The k-fold cross validation is performed using the `Scikit-learn` Python code. The optimization process stops when the MSE is less than a threshold  $\epsilon = 10^{-5}$ .

**Optimization process :** Several optimization studies can be performed using `Scipy` [8] for classical optimization techniques (such as Nelder-Mead technique). The `Deap` Python optimization library [37] has been applied for optimization using the genetic algorithm (GA) technique. For the multi-objective optimization study, the NSGA-II [15] is used to obtain the Pareto front. The `Matplotlib` Python plotting library has been used for plotting.

### 3 Results and discussion

#### 3.1 The training dataset

Figure 3 presents a scatter plot for the training data set. The training dataset has been created using the Box-Behnken design of experiment (DoE) [7] and has been used in a previous study to optimize the cyclone geometry using the polynomial regression and radial basis function artificial neural network surrogates [26]. The minimum and maximum values for the four design parameters are listed in Table 3. To avoid scaling effect, all values are scaled (using the `preprocessing.MinMaxScaler` class from `Scikit-learn`) to be in range of 0 to 1 before being used in training the surrogates.

It is worth to mention that the Box-Behnken design of experiments [7] are widely used sampling plan to fit a multi-dimensional polynomial (including interactions) [58]. This sampling plan is known as space-filling. It requires uniform spread of points, consequently it leaves a gap in the projections [36]. Latin hypercube sampling (LHS) [56] is a better alternative to the stratified sampling plan [31]. This means the given training data to the SVR is not the best for testing the SVR, so we consider this as a severe test for the SVR meta models. In future studies a new data set based on LHS will be created whereas the current one will be used for testing.

The variation of the two performance parameters (Euler and Stokes numbers) are shown in Fig. 4 for the 33 (27 from the DoE and 6 extra cases) test cases (cf. Table 10,

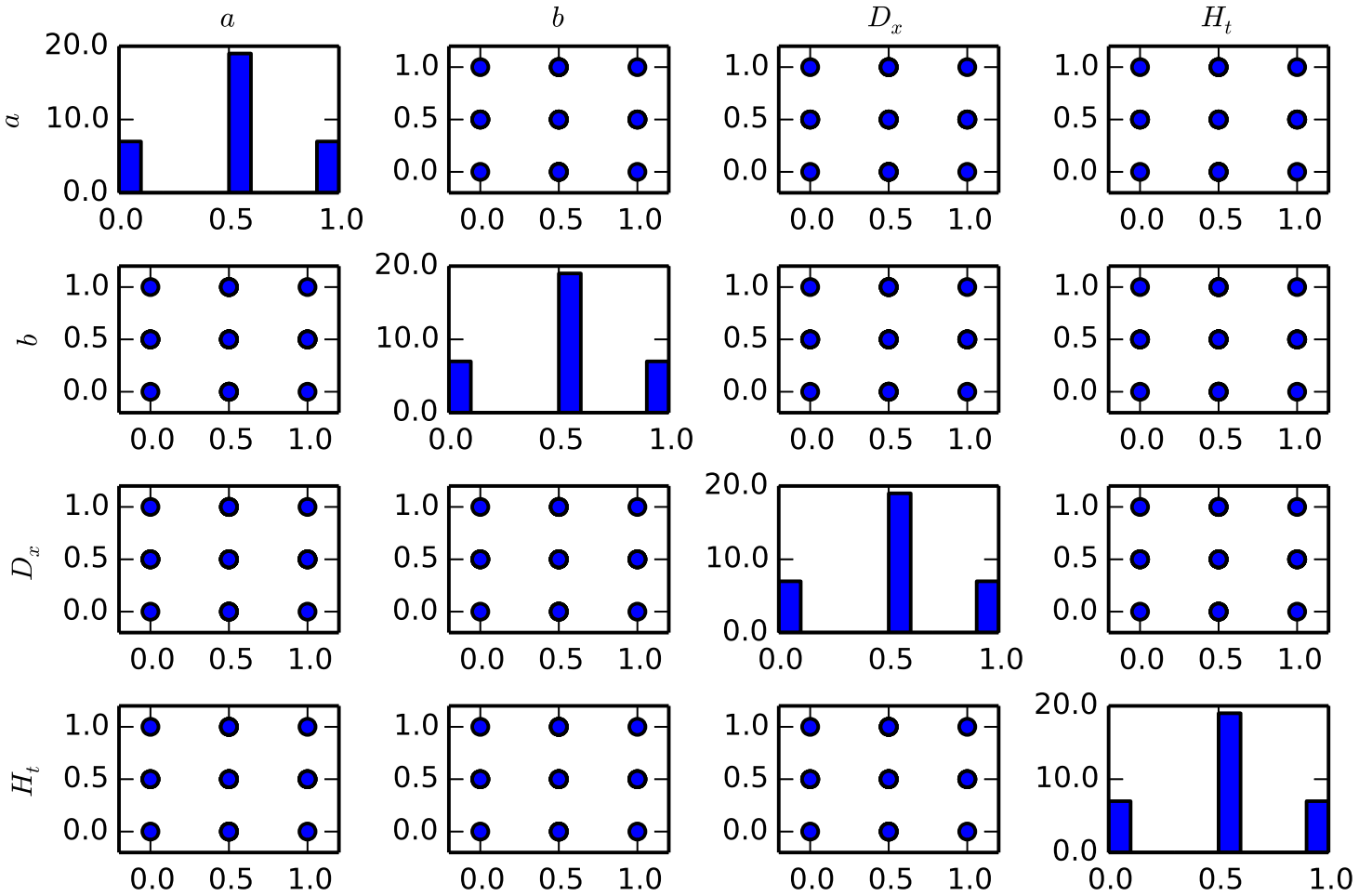


Figure 3: Scatter plot for the training dataset generated using the Box-Behnken DoE (scaled from 0 to 1).

Table 3: The values of the cyclone geometrical parameters used in the DoE (cf. Fig. 1)

Variables	Minimum	Center	Maximum
Inlet height, $x_1 = a/D$	0.4	0.55	0.7
Inlet width, $x_2 = b/D$	0.14	0.27	0.4
Vortex finder diameter, $x_3 = D_x/D$	0.2	0.475	0.75
Total cyclone height, $x_4 = H_t/D$	3.0	5.0	7.0
Cylinder height, $h/D$		1.5	
Vortex finder length, $S/D$		0.5	
Cone-tip diameter, $B_c/D$		0.375	

The values of the cylinder height, vortex finder length and the cone tip diameters are kept at the Stairmand design values, where  $h - S = 1$  which is the optimum difference between the two dimensions as reported by many researchers [27]

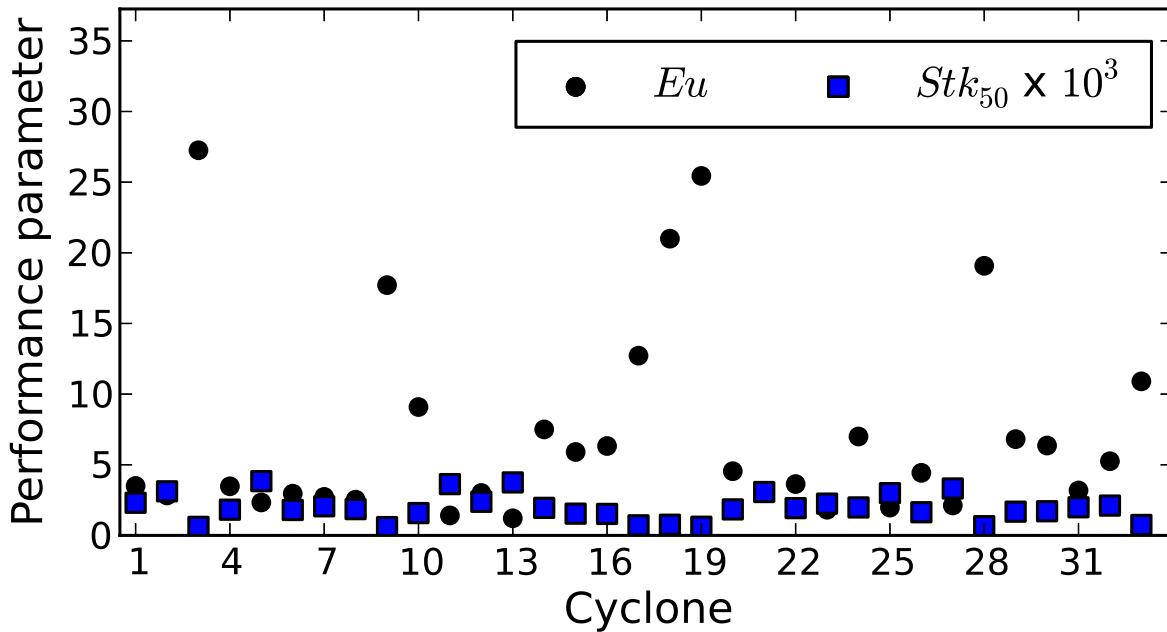


Figure 4: The variation of the cyclone performance from cyclone to cyclone.

p. 258 in Elsayed and Lacor [30]).

Table 4 presents the statistical descriptive parameters for the SVR (before and after parameter optimization) and Kriging surrogate. It is clear that the SVR with optimized parameter superior the performance of the Kriging model as is clear from the better matching between the statistical descriptive parameters of the input and the output results from the surrogate as well as the smaller value of MSE and the  $R^2$  value close to unity.

Table 4: Statistical descriptive parameters for the SVR and KG models using the 5-fold cross validation\*

SVR before parameter optimization (using the default values of $C$ and $\gamma$ )				
	Eu		$Stk_{50} \times 10^3$	
	x	y	x	y
Average	7.2436	4.3035	1.9496	1.9404
Standard deviation	6.9465	1.1746	0.9211	0.7573
Minimum	1.2110	2.0240	0.5880	0.6646
Maximum	27.2570	6.5702	3.8400	3.2680
Range	26.0460	4.5462	3.2520	2.6035
<b>Coefficient of determination, <math>R^2</math></b>		0.131		0.900
<b>Mean squared error</b>		47.750		0.076
Intercept		3.2928		0.3480
Slope		0.1395		0.8168
The SVR regularization parameter, $C$		10.0		10.0
The kernel parameter, $\gamma$		10.0		10.0

SVR after parameter optimization				
	Eu		$Stk_{50} \times 10^3$	
	x	y	x	y
Average	7.2436	7.2966	1.9496	1.9938
Standard deviation	6.9465	6.9108	0.9211	0.9271
Minimum	1.2110	1.3118	0.5880	0.4882
Maximum	27.2570	27.1573	3.8400	3.7398
Range	26.0460	25.8455	3.2520	3.2517
<b>Coefficient of determination, <math>R^2</math></b>		0.9991		0.9941
<b>Mean squared error</b>		2.579		0.00883
Intercept		0.0935		0.0372
Slope		0.9944		1.0036
The SVR regularization parameter, $C$		13502		283.151
The kernel parameter, $\gamma$		0.154		0.041

Kriging (KG)				
	Eu		$Stk_{50} \times 10^3$	
	x	y	x	y
Average	7.2436	7.2436	1.9496	1.9496
Standard deviation	6.9465	6.9465	0.9211	0.9211
Minimum	1.2110	1.2110	0.5880	0.5880
Maximum	27.2570	27.2570	3.8400	3.8400
Range	26.0460	26.0460	3.2520	3.2520
<b>Coefficient of determination, <math>R^2</math></b>		0.876		0.999
<b>Mean squared error</b>		5.506		0.001
Intercept		0.0		0.0
Slope		1.0		1.0

\* x is the input to the SVR and y is the predicted value. Both x and y represent the Euler number and Stokes number.

Note that the values of *the average, the standard deviation, the minimum, the maximum and the range* have been calculated using all data for training the meta model. Consequently, for Kriging interpolation metamodel, these values are identical for x and y columns.

The average coefficient of determination  $R^2$  using cross validation can be calculated as  $R^2 = \frac{1}{K} \sum_{j=1}^K \left( 1 - \frac{SS_{res_j}}{SS_{tot_j}} \right)$  where  $K$  is the number of folds,  $SS_{res_j} = \sum_{i=1}^{Nt_j} (y_i - \hat{y}_i)^2$  is the sum of squares of residuals,  $SS_{tot_j} = \sum_{i=1}^{Nt_j} (y_i - \bar{y}_j)^2$  is the total sum of squares,  $Nt_j$  is the number of testing points in fold  $j$ ,  $y_i$  represents the actual values,  $\bar{y}_j = \frac{1}{Nt_j} \sum_{i=1}^{Nt_j} y_i$  is the mean of the observed data in fold  $j$  and  $\hat{y}_i$  represent the predicted values.

Q-Q plot is a plot of the percentiles (or quintiles) of a standard normal distribution against the corresponding percentiles of the observed (given) untrained data. If the observations follow approximately a normal distribution or the two compared datasets are of the same statistical distribution, *the resulting plot should be roughly a straight line with a positive slope*. Deviations from this would indicate possible departures from a normal distribution or the two datasets belonging to different statistical distributions. The ob-

tained Q-Q plot is linear (a straight diagonal line) for the SVR models with optimized parameters as shown in Table 5. Whereas the Q-Q plot shape of distribution appears to be left skewed and right skewed in case of Stokes number and the Euler number values respectively predicted by the traditional SVR. This indicates that the traditional SVR (without parameter optimization) model is less accurate model with respect to the SVR with optimized parameters. The interested reader can refer to [50] and the Matlab statistics toolbox user's guide [55] for more details about the Q-Q plot.

It is clear that the accuracy of the surrogate model has been increased due to parameter optimization. Moreover, the linear fit for the input-output relationship has been enhanced by optimizing the SVR parameters.

### 3.2 Geometry effect

One of the benefit of using surrogate models is to apply them to study the effect of each design variable on the response (performance parameters). The two optimized SVR models are used to study the effect of the four geometrical parameters on both the Euler number and the Stokes number. As is clear from Fig. 5, the SVR and KG models give the same trend of variation but the SVR models can predict more local variation than the KG model. It is worth to mention that the variation of the Euler number with the change in the vortex finder diameter  $D_x$  predicted by the SVR model is similar to that reported by the authors in previous studies [20, 26]. For the variation of the cyclone performance with the total height ( $H_t$ ), the reduction in the Euler number (pressure drop) stops after  $H_t = 4.625$  whereas the enhancement in the collection efficiency (reduction in the cut-off diameter) continue with lengthen the cyclone.

The highly non-linear relationship between the two performance parameters and the four geometrical parameters can be understood in a deeper way by inspecting the 3D plots presented in Fig. 6. The following conclusions are drawn from the analysis of Fig. 6. There is clear interaction between the four geometrical parameters. The sensitivity of the Euler number to the change of the geometry is much more than that of the Stokes number.

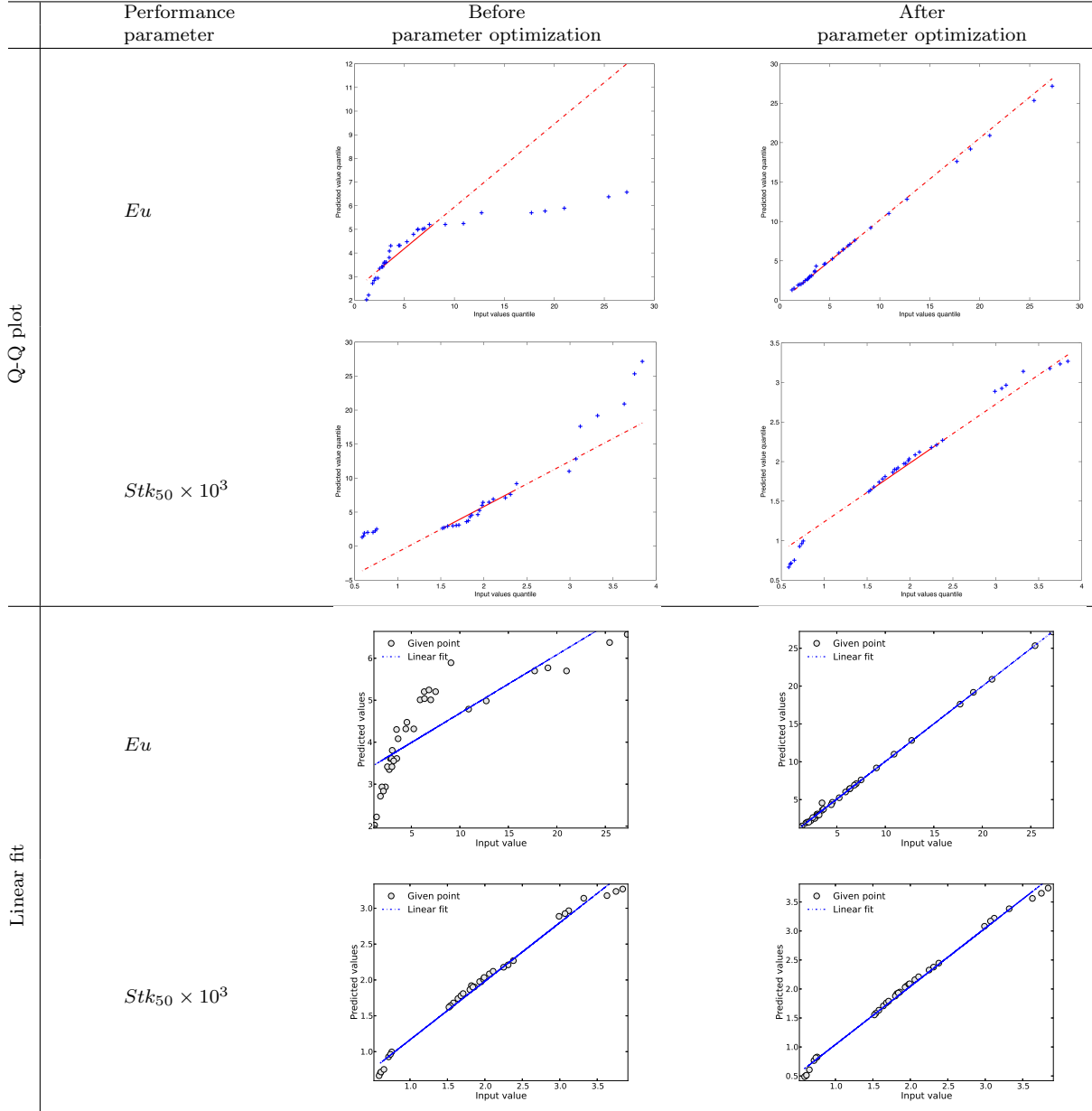
### 3.3 Geometry optimization

Two optimization techniques have been applied to obtain new geometrical ratio set, namely the Nelder-Mead technique [59] and the genetic algorithms [25, 46]. Table 6 lists the new generated cyclone geometry ratios for minimum pressure drop (Euler number).

For single objective and one parameter optimization using the Nelder-Mead technique from `Scipy`. The total cyclone height  $H_t$  is optimized for minimum Euler number. The optimum value of  $H_t$  is 4.694, i.e.,  $h_c = 3.194$ , where  $h = 1.5$  which results in  $Eu = 3.432$ .

Since the cyclone performance has two major performance indices (the Euler and the

Table 5: Q-Q plots and the input-output linear fit before and after parameter optimization (using all data points for training)



Stokes numbers) a multi-objective optimization process is needed for optimum cyclone performance. In this study, NSGA-II [15, 26] available from `deep` (evolutionary toolbox for python) [37] has been used to obtain the Pareto front shown in Fig. 7 and Table 7.

The obtained Pareto front has been used to fit a correlation between the two performance parameters. The application of the `polyfit` function from Numpy Python package

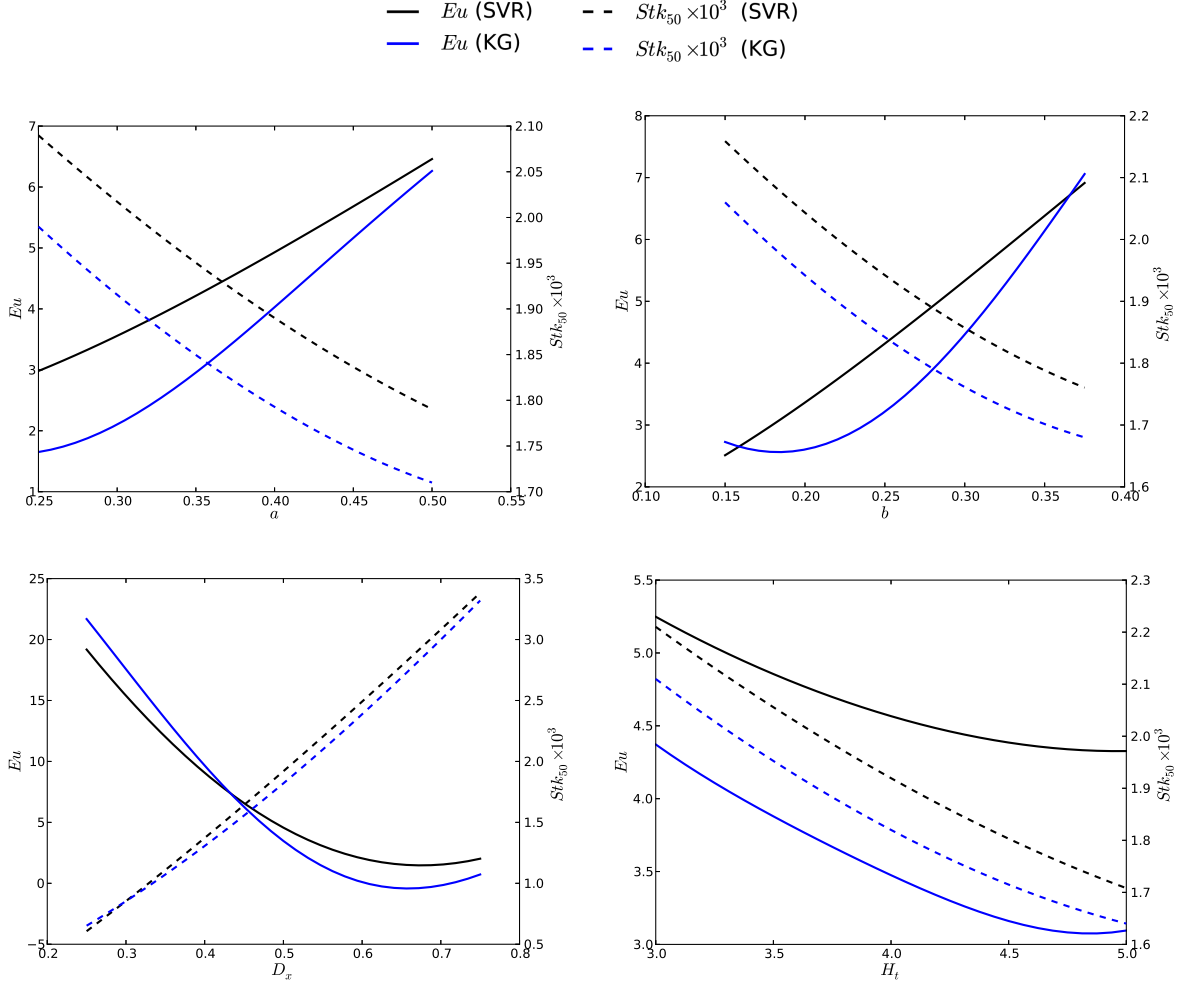


Figure 5: Comparison between the effect of each geometrical parameter on the cyclone performance parameters using SVR (black lines) and KG (blue lines).

[8] results in the following correlation  $Stk_{50} \times 10^3 = 10^{-0.065z^3 - 0.195z^2 - 0.193z + 0.372}$  where  $z = \log_{10}(Eu)$ . It is worth to mention that the accuracy of the new third order correlation is  $R^2 = 0.996$  which is superior that proposed by the authors in a previous article [25]. This correlation can be used to predict the Stokes number (the cut-off diameter) given the pressure drop (Euler number).

Table 6: Optimum geometrical ratios for minimum Euler number

	<i>a</i>	<i>b</i>	<i>D<sub>x</sub></i>	<i>H<sub>t</sub></i>	<i>Eu</i>
Optimum cyclone total height (Nelder-Mead technique)	0.25	0.15	0.5	4.694	3.432
Optimization of the four factors (Nelder-Mead technique)	0.499	0.15	0.658	3.0	0.667



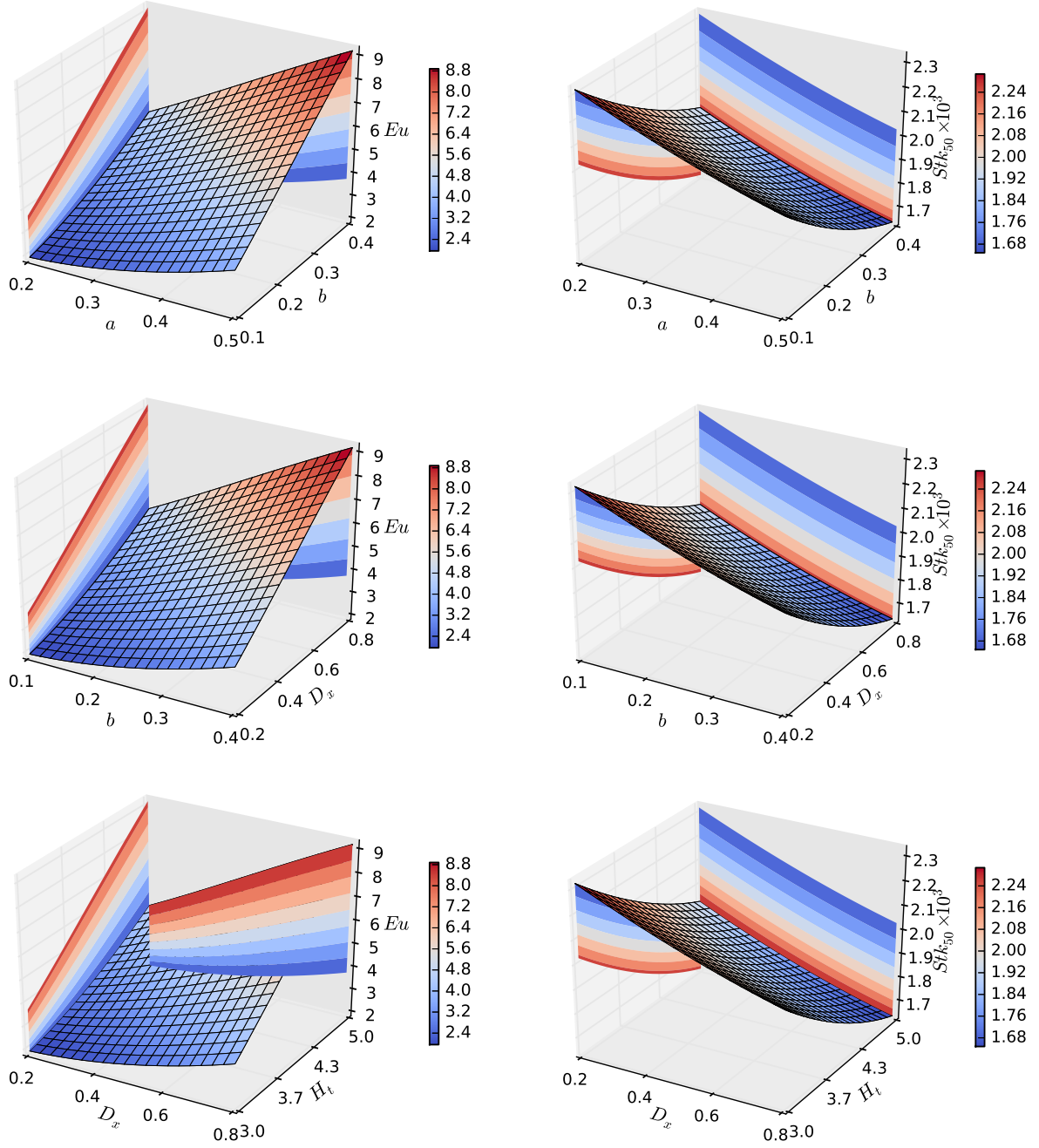


Figure 6: Surface plots for the effect of each geometrical parameter on the cyclone performance parameters using SVR

Table 7: The Pareto-Front points and the corresponding geometrical parameters values

$a$	$b$	$D_x$	$H_t$	$Eu$	$Stk_{50} \times 10^3$
0.302	0.238	0.643	4.103	0.193	2.590
0.284	0.246	0.572	4.229	0.622	2.420
0.294	0.246	0.546	4.484	1.170	2.200
0.298	0.239	0.520	4.529	1.690	2.050
0.318	0.241	0.501	4.479	2.330	1.920
0.265	0.240	0.471	4.549	2.630	1.820
0.259	0.230	0.435	4.601	3.490	1.650
0.275	0.241	0.440	4.992	4.140	1.570
0.251	0.215	0.396	4.831	4.690	1.450
0.250	0.215	0.363	4.772	5.700	1.290
0.253	0.219	0.349	4.991	6.570	1.180
0.250	0.203	0.319	4.940	7.310	1.070
0.250	0.203	0.302	4.940	7.940	0.993
0.255	0.151	0.266	5.000	8.730	0.918
0.255	0.169	0.250	4.999	9.580	0.802
0.255	0.193	0.250	4.999	10.100	0.755
0.251	0.232	0.250	5.000	11.100	0.691
0.273	0.244	0.250	4.995	12.400	0.641
0.294	0.245	0.250	5.000	13.300	0.612
0.306	0.266	0.250	4.992	14.800	0.566
0.319	0.273	0.250	5.000	15.800	0.537
0.359	0.273	0.250	4.996	17.700	0.491
0.346	0.306	0.250	4.996	18.900	0.468
0.381	0.300	0.250	4.994	20.300	0.437
0.402	0.308	0.250	4.963	21.800	0.411
0.420	0.331	0.250	5.000	24.100	0.373
0.464	0.340	0.250	5.000	26.700	0.336
0.500	0.351	0.251	5.000	28.900	0.313

### 3.4 CFD comparison between the Stairmand and optimal design

In order to understand the flow pattern of the optimum points, the Pareto front point which produces the minimum Euler number has been simulated and compared with the Stairmand design. The Reynolds stress turbulence model has been used to model the turbulent flow in the two cyclone separators. For the detailed governing equation for the Reynolds averaged Navier-Stokes equation (RANS) we refer to Elsayed and Lacor [21]. The geometrical values are given in Table 8 for the two cyclones (cf. Fig. 8).

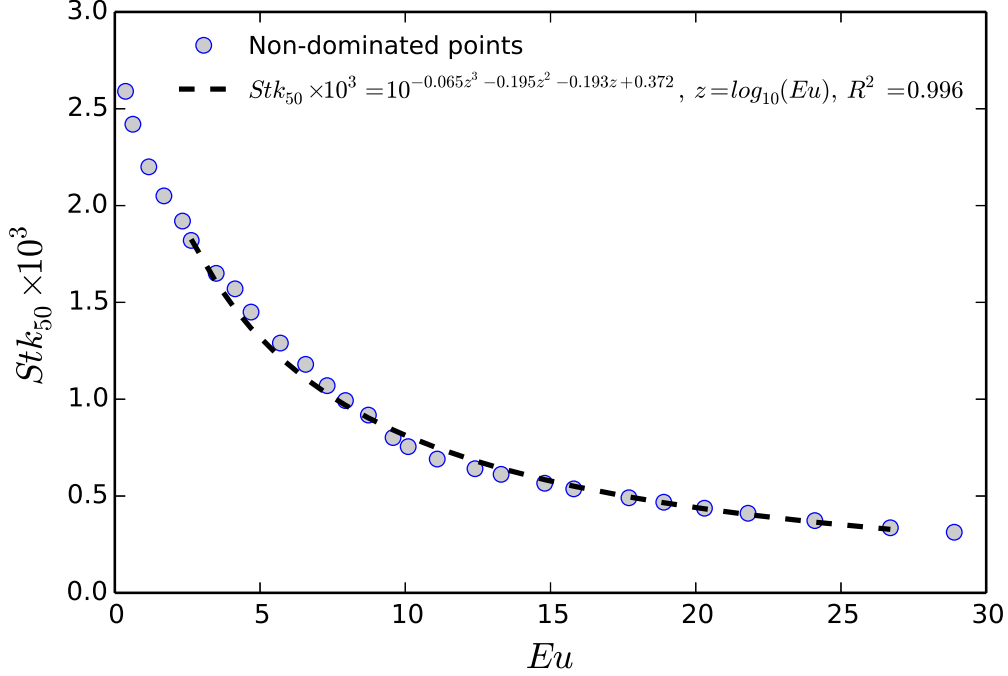


Figure 7: Pareto front for NSGA-II optimization with polynomial fit

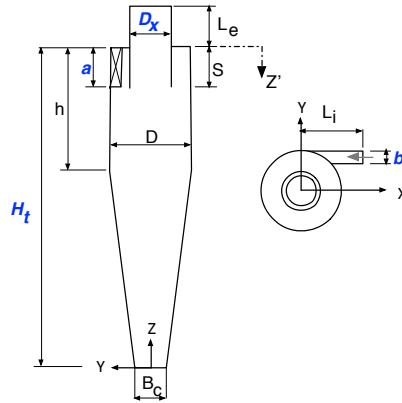
The air volume flow rate  $Q_{in}=50$  l/min for the two cyclones, air density is  $1.0$   $kg/m^3$  and dynamic viscosity  $2.11 \times 10^{-5}$  Pa.s. The turbulent intensity equals 5% and characteristic length equals 0.07 times the inlet width [43]. A velocity inlet boundary condition is applied at inlet, outflow at gas outlet and wall boundary conditions at all other boundaries [26].

The finite volume method has been used to discretize the partial differential equations of the model using the SIMPLEC (Semi-Implicit Method for Pressure-Linked Equations-Consistent) method for pressure velocity coupling and QUICK scheme to interpolate the variables on the surface of the control volume. The implicit coupled solution algorithm was selected. The unsteady Reynolds stress turbulence model (RSM) was used in this study with a time step of 0.0001s.

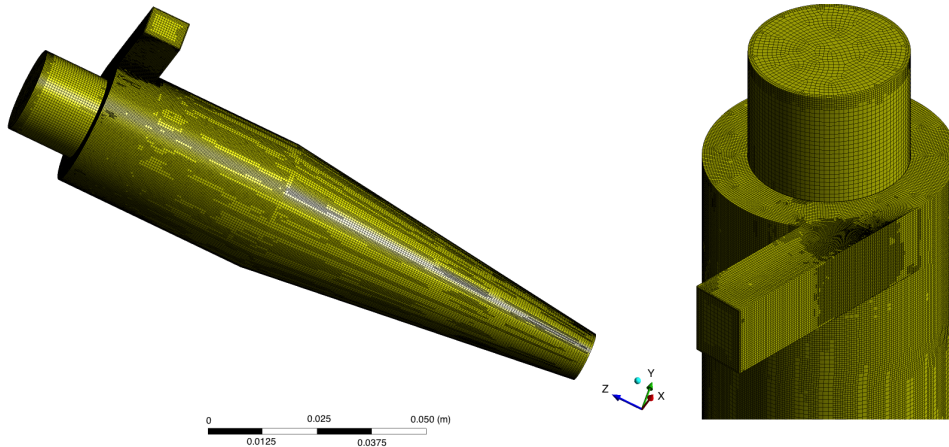
The grid independence study has been performed for the tested cyclones. Three levels of grid for each cyclone have been tested, to be sure that the obtained results are grid independent. The hexahedral computational grids were generated using Gambit grid generator and the simulations were performed using Ansys Fluent 15 commercial finite

 Table 8: The values of geometrical parameters for the two designs ( $D=31 \times 10^{-3}$  m)

Cyclone	$a/D$	$b/D$	$D_x/D$	$H_t/D$	$h/D$	$S/D$	$B_c/D$	$L_i/D$	$L_e/D$
Stairmand design	0.5	0.2	0.5	4	1.5	0.5	0.375	1.0	0.5
New design	0.302	0.238	0.643	4.103	1.5	0.5	0.375	1.0	0.5



(a) The cyclone geometry



(b) The surface mesh for the new design.

Figure 8: The cyclone geometry and the surface mesh for the new design.

volume solver on a four nodes CPU Opteron 64 Linux cluster.

In this study, we applied the approach proposed by Elsayed et al. [32, 33] for mesh independence study. Where the adjoint solver is used to locally refine the mesh at the region of high gradient. The fine mesh for the optimum design is shown in Fig. 8. The mesh is locally refined twice at the region of high pressure drop using the adjoint solver. The details of the grid independence study using grid convergence index (GCI) is shown in Table 9. For more details about GCI approach and the grid independence study for the Stairmand cyclone we refer to Elsayed and Lacor [26]. In the current study, the CFD results on the fine mesh are presented. The value of  $\alpha = 1.0976$  is close to unity indicates that the change is in the asymptotic range. A qualitative representation of the

Table 9: Grid convergence calculations using GCI method and three grid levels for the Euler number

$i$	$N_i$	$Eu_i$	$r_{i,i+1}$	$e_{i,i+1}$	$\varepsilon_{i,i+1}$	$GCI_{i,i+1}^{\text{fine}}$	$R^a$	$\alpha^b$
$0^c$		0.1634						
1	1002171	0.2050						
			1.0413	0.0200	0.0976	25.3674		
2	887480	0.2250					0.0822	1.0976
			1.1886	0.2670	1.1867	34.2236		
3	528499	0.4920						

<sup>a</sup>  $R = \varepsilon_{12} / \varepsilon_{23}$ .

<sup>b</sup>  $\alpha = (r_{12}^p GCI_{12}) / GCI_{23}$ .

<sup>c</sup> The value at zero grid space ( $h \rightarrow 0$ ).  $i=1, 2$  and  $3$  denote the calculations at the fine, medium and coarse mesh respectively.

grid independence study for the new design is shown in Fig. 9.

In order to validate the obtained results, it is necessary to compare the prediction with experimental data. Such comparison has been published before in previous articles [21, 24, 26]. That comparison was performed with the measurements of Hoekstra [42, 65] using the Laser Doppler anemometry (LDA) technique for both the axial and tangential velocity profiles. Moreover, the numerical results for the pressure drop have been compared with the corresponding experimental values [21]. The validation showed an acceptable matching between the simulation results and the experimental values.

### 3.4.1 Flow field pattern and performance

All the subsequent figures present the flow variables in a dimensionless form. This approach results in a better study how the velocity varies inside the cyclone in terms of the average inlet velocity. Moreover, This allows to compare the velocity profiles for different cyclones working at different inlet velocities (at a fixed volume flow rate). The dimensional value of the velocity can be calculated using the given volume flow rate and the inlet section dimensions. In case of static pressure, the pressure value can be estimated using the dynamic pressure at the inlet ( $\frac{1}{2}\rho V_{in}^2$ ), where  $\rho$  is the gas density,  $V_{in}$  is the average inlet velocity. The approach of representing the velocity and pressure profiles in dimensionless forms is widely used in the cyclone separator studies e.g., Derksen et al. [17, 18], Gronald and Derksen [41].

Figures 10 and 11 show the contour plot at the mid plane  $Y=0$  and throughout the mid of the inlet section respectively. In the two cyclones, the time-averaged dimensionless static pressure decreases radially from the wall to center. A negative pressure zone appears in the forced vortex region (central region) due to high swirling velocity. The pressure gradient is large along the radial direction, whereas the gradient in the axial direction

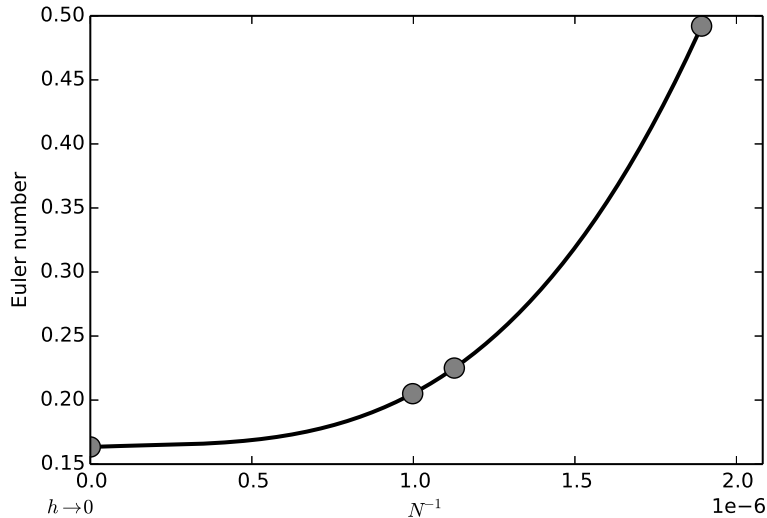


Figure 9: Qualitative representation of the grid independence study. The Euler number for the optimum design using the three grid levels.  $N^{-1}$  is the reciprocal of the number of cells,  $h \rightarrow 0$  means the value at zero grid size (cf. Table 9).

is very limited (cf. Fig. 12). The cyclonic flow is not symmetrical as is clear from the shape of the low-pressure zone at the cyclone center (twisted cylinder). However, the two cyclones have almost the same flow pattern, but the static pressure of the Stairmand design is nearly eight folds that of the new design. If we used the same color ranges for the two cyclones, the radial variations in the new design will be difficult to be distinguished. The contour plots at the inlet section (Fig. 11) show that the pressure distribution in the vortex finder is almost uniform in the new design. Whereas, the Stairmand design keep the same radial variation throughout the cyclone. The pressure distribution around the vortex finder in the new design is more uniform with respect to that for the Stairmand design. Due to flow acceleration (with reduced area) at the inlet, a negative pressure zone is established in the new design. The dimensionless static pressure distribution presented in Fig. 13 for the two cyclones indicates that the highest dimensionless static pressure for the Stairmand design is more than eight times that of the new design at all sections (due to limited axial variations). This indicates that, the new design has a lower pressure drop than the Stairmand design. However, these results are obtained at different inlet velocity for the two cyclones (to have the same air flow rate). The same Euler number values would be obtained if the two cyclones work at the same inlet velocity because the Euler number is not a function of flow velocity if the Reynolds number is higher than  $2 \times 10^4$  [20].

The tangential velocity profile is composed of two regions. In the inner region, the flow rotates approximately like a solid body (forced vortex), where the tangential velocity increases with radius. After reaching its peak the velocity decreases with radius in the

Table 10: The predicted Euler number for the two designs

Design	CFD simulation	Support vector regression
Stairmand	5.606	5.783 ( $Stk_{50} \times 10^3 = 1.913$ )
New design	0.205	0.193 ( $Stk_{50} \times 10^3 = 2.590$ )

outer part of the profile (free vortex). The tangential velocity distributions for the two cyclones are nearly identical in pattern (Rankine profile). The inner part of the tangential velocity distribution of the two cyclones exhibit the weak vortex (new design) versus the strong vortex (Stairmand design). The outer part for the new design is shorter in comparison with the Stairmand cyclone. This implies that the particles in the Stairmand cyclone will be subjected to higher centrifugal force with respect to that in the new design. The maximum dimensionless tangential velocity for Stairmand cyclone is higher than twice that for the new design. The cyclone collection efficiency is affected by the maximum tangential velocity and the separation space. Since, the two cyclones have close values for the cyclone volume, the expected collection efficiency from the Stairmand cyclone (designed for high-efficiency) is much higher than that for the new design (optimized for low-pressure loss). From the inspection of the contour plots at the inlet section, the vortex strength highly reduced upon entering the separation space in case of the new design. This is also clear when the tangential velocity contours for the two cyclones are colored using the same color ranges (Fig. 10).

The axial velocity in the inner vortex is either reported as an inverted V or inverted W-shaped profile, i.e., with a maximum (V-shaped) or a dip (W-shaped) at the symmetry axis [13, 47]. The axial velocity profiles for the Stairmand design is the inverted W profile. Whereas the new design exhibit the inverted V profile (Fig. 10). However, the axial variation of the axial velocity is limited in the two cyclones as is clear from Fig. 12, the maximum axial velocity increases as we move to the gas exit. The relatively small axial velocity (in addition to the relatively small tangential velocity) in the new design, will reduce the possibility of the re-entrainment of the collected particle. The radial variation of the axial velocity in the Stairmand design is larger than that in the new design.

Table 10 compares the Euler number values fro the two designs. The CFD simulation results estimated the pressure drop of the Stairmand cyclone as 27 times that for the new design, whereas the support vector regression model gives 30 ( $Eu_{\text{Stairmand design}}/Eu_{\text{new design}}$ ). On the other hand, the ratio of the predicted stokes number for the new design is 1.35 times that for the Stairmand design. This implies that the new design will be preferable for relatively larger particle than that for the Stairmand cyclone.

## 4 Conclusions

In order to accurately predict the complex non-linear relationships between the cyclone performance parameters and its geometrical dimensions, the support vector machines approach has been used and compared with the Kriging surrogate. Two support vector regression (SVR) surrogate models have been trained and tested by 33 CFD data sets. The result demonstrates that SVR can offer an alternative and powerful approach to model the performance parameters. The SVR model parameters have been optimized to obtain the most accurate results from the cross validation steps. The parameters optimization has been optimized using the Simulated annealing technique. SVR (with optimized parameters) can offer an alternative and powerful approach to model the performance parameters better than Kriging. The SVR surrogates used to study the effect of the four geometrical parameters on the cyclone performance. The genetic algorithms optimization technique has been used to obtain a new geometrical ratio for minimum Euler number and for minimum Euler and Stokes numbers. The new cyclones over-perform the standard Stairmand design performance. A table for Pareto front is provided where the decision-maker can select from. A new correlation between the Stokes number and Euler number is provided which is more accurate than the existing correlations in the literature.

CFD simulations for the Stairmand design and the new design for minimum Euler numbers are performed using the Reynolds stress turbulence model. The analysis of the CFD results reveal the changes in the flow field pattern which cause the better performance (less pressure drop) presented by the new design.

## References

- [1] Alexander, R. M., 1949. Fundamentals of cyclone design and operation. In: Proceedings of the Australian Institute of Mineral and Metallurgy. No. 152. pp. 203–228.
- [2] Asl, A. N., Menhaj, M. B., Sajedin, A., 2014. Control of leader–follower formation and path planning of mobile robots using asexual reproduction optimization (aro). *Applied Soft Computing* 14, Part C (0), 563 – 576.  
URL <http://www.sciencedirect.com/science/article/pii/S1568494613002883>
- [3] Avci, A., Karagoz, I., 1 2001. Theoretical investigation of pressure losses in cyclone separators. *International Communications in Heat and Mass Transfer* 28 (1), 107–117.
- [4] Ayat, N.-E., Cheriet, M., Suen, C. Y., 2005. Automatic model selection for the optimization of svm kernels. *Pattern Recognition* 38 (10), 1733–1745.
- [5] Barth, W., 1956. Design and layout of the cyclone separator on the basis of new investigations. *Brennstow-Wärme-Kraft (BWK)* 8 (4), 1–9.



- [6] Baylar, A., Hanbay, D., Batan, M., 2009. Application of least square support vector machines in the prediction of aeration performance of plunging overfall jets from weirs. *Expert Systems with Applications* 36 (4), 8368–8374.
- [7] Box, G., Behnken, D., 1960. Some new three level designs for the study of quantitative variables. *Technometrics* 2, 455–475.
- [8] Bressert, E., 2012. *SciPy and NumPy: An Overview for Developers*. O’Reilly Media.
- [9] Casal, J., Martinez-Benet, J. M., 1983. A better way to calculate cyclone pressure drop. *Chemical Engineering* 90 (2), 99–100.
- [10] Chen, J., Shi, M., 2007. A universal model to calculate cyclone pressure drop. *Powder Technology* 171 (3), 184 – 191.
- [11] Chen, N., Lu, W., Yang, J., Li, G., 2004. *Support vector machine in chemistry*. World Scientific.
- [12] Chuah, T. G., Gimbut, J., Choong, T. S., 2006. A CFD study of the effect of cone dimensions on sampling aerocyclones performance and hydrodynamics. *Powder Technology* 162, 126 – 132.
- [13] Cortés, C., Gil, A., 2007. Modeling the gas and particle flow inside cyclone separators. *Progress in Energy and Combustion Science* 33 (5), 409 – 452.
- [14] De Souza, F. J., Salvo, R. D. V., Martins, D. A. D. M., 2012. Large eddy simulation of the gas-particle flow in cyclone separators. *Separation and Purification Technology* 94, 61–70.
- [15] Deb, K., Pratap, A., Agarwal, S., Meyarivan, T., 2002. A fast and elitist multiobjective genetic algorithm: NSGA-II. *IEEE Transaction Evolutionary Computation* 6, 182–197.
- [16] Derksen, J., 2003. Les of swirling flow in separation devices. In: *Proceedings of the 3rd International Symposium on Turbulence and Shear Flow Phenomena Sendai, Japan*. pp. 911–916.
- [17] Derksen, J. J., Sundaresan, S., van den Akker, H. E. A., 2006. Simulation of mass-loading effects in gas–solid cyclone separators. *Powder Technology* 163, 59–68.
- [18] Derksen, J. J., van den Akker, H. E. A., Sundaresan, S., 2008. Two-way coupled large-eddy simulations of the gas-solid flow in cyclone separators. *AIChE Journal* 54 (4), 872–885.
- [19] Dirgo, J., 1988. *Relationship between cyclone dimensions and performance*. Ph.D. thesis, Harvard University, USA.

- [20] Elsayed, K., Lacor, C., 2010. Optimization of the cyclone separator geometry for minimum pressure drop using mathematical models and CFD simulations. *Chemical Engineering Science* 65 (22), 6048–6058.
- [21] Elsayed, K., Lacor, C., 2011. The effect of cyclone inlet dimensions on the flow pattern and performance. *Applied Mathematical Modelling* 35 (4), 1952–1968.
- [22] Elsayed, K., Lacor, C., 2011. Modeling, analysis and optimization of aircyclones using artificial neural network, response surface methodology and CFD simulation approaches. *Powder Technology* 212 (1), 115–133.
- [23] Elsayed, K., Lacor, C., 2011. Numerical modeling of the flow field and performance in cyclones of different cone-tip diameters. *Computers & Fluids* 51 (1), 48–59.
- [24] Elsayed, K., Lacor, C., 2012. The effect of the dust outlet geometry on the performance and hydrodynamics of gas cyclones. *Computers & Fluids* 68, 134–147.
- [25] Elsayed, K., Lacor, C., 2012. Modeling and pareto optimization of gas cyclone separator performance using RBF type artificial neural networks and genetic algorithms. *Powder Technology* 217, 84 – 99.
- [26] Elsayed, K., Lacor, C., 2013. CFD modeling and multi-objective optimization of cyclone geometry using desirability function, artificial neural networks and genetic algorithms. *Applied Mathematical Modelling* 37 (8), 5680–5704, <http://dx.doi.org/10.1016/j.apm.2012.11.010>.
- [27] Elsayed, K., Lacor, C., 19-21 December 2013. Comparison of Kriging, RBFNN, RBF and polynomial regression surrogates in design optimization. In: Eleventh International Conference of Fluid Dynamics (ICFD11). Alexandria, Egypt.
- [28] Elsayed, K., Lacor, C., 2013. The effect of cyclone vortex finder dimensions on the flow pattern and performance using LES. *Computers & Fluids* 71, 224 – 239.
- [29] Elsayed, K., Lacor, C., 19-21 December 2013. Robust parameter design optimization using Kriging, RBF and RBFNN. In: Eleventh International Conference of Fluid Dynamics (ICFD11). Alexandria, Egypt.
- [30] Elsayed, K., Lacor, C., 2014. CFD-Based Analysis and Optimization of Gas Cyclones Performance. International Energy and Environment Foundation (IEEF), ISBN 13: 978-1-49487-575-6, Ch. 8, pp. 223–276.
- [31] Elsayed, K., Lacor, C., 27-29 May 2014. Optimization of multi-fidelity data using Co-Kriging for high dimensional problems. In: 16th International Conference on Applied Mechanics and Mechanical Engineering (AMME-16). The Military Technical College, Cairo, Egypt.

- [32] Elsayed, K., Miranda, J., Ghorbaniasl, G., Lacor, C., 27-29 May 2014. 2D viscous shape design optimization and mesh adaptation using the adjoint method. In: 16th International Conference on Applied Mechanics and Mechanical Engineering (AMME-16). The Military Technical College, Cairo, Egypt.
- [33] Elsayed, K., Miranda, J., Ghorbaniasl, G., Lacor, C., 4-6 June 2014. Optimal cyclone geometry using the adjoint methods. In: Papadrakakis, M., Karlaftis, M., Lagaros, N. (Eds.), *OPT-i An International Conference on Engineering and Applied Sciences Optimization*. Kos Island, Greece.
- [34] Elsayed, K., Vucinic, D., D'Ippolito, R., Lacor, C., 2012. Comparison between RBF and kriging surrogates in design optimization of high dimensional problems. In: EngOpt2012, 3rd International Conference on Engineering Optimization, Rio de Janeiro, Brazil, 1-5 July.
- [35] First, M. W., 1949. Cyclone dust collector design. ASME Annual General Meeting, Paper No. 49A127.
- [36] Forrester, A. I. J., Sobester, A., Keane, A. J., 2008. *Engineering design via surrogate modelling: A practical guide*. J. Wiley, Chichester, West Sussex, England.
- [37] Fortin, F.-A., De Rainville, F.-M., Gardner, M.-A., Parizeau, M., Gagne, C., 2012. Deap: Evolutionary algorithms made easy. *Journal of Machine Learning Research* 13, 2171 – 2175.
- [38] Gimbut, J., Chuah, T., Fakhru'l-Razi, A., Choong, T. S. Y., 2005. The influence of temperature and inlet velocity on cyclone pressure drop: a CFD study. *Chemical Engineering & Processing* 44 (1), 7–12.
- [39] Gimbut, J., Chuah, T. G., Choong, T. S. Y., Fakhru'l-Razi, A., 2005. A CFD study on the prediction of cyclone collection efficiency. *International Journal for Computational Methods in Engineering Science and Mechanics* 6 (3), 161 – 168.
- [40] Griffiths, W. D., Boysan, F., 1996. Computational fluid dynamics (CFD) and empirical modelling of the performance of a number of cyclone samplers. *Journal of Aerosol Science* 27 (2), 281–304.
- [41] Gronald, G., Derksen, J. J., 2011. Simulating turbulent swirling flow in a gas cyclone: A comparison of various modeling approaches. *Powder Technology* 205 (1-3), 160 – 171.
- [42] Hoekstra, A. J., 2000. Gas flow field and collection efficiency of cyclone separators. Ph.D. thesis, Technical University Delft.

- [43] Hoekstra, A. J., Derksen, J. J., Van Den Akker, H. E. A., 1999. An experimental and numerical study of turbulent swirling flow in gas cyclones. *Chemical Engineering Science* 54, 2055–2065.
- [44] Hoffmann, A., De Groot, M., Hospers, A., August 1996. The effect of the dust collection system on the flow pattern and separation efficiency of a gas cyclone. *The Canadian Journal of Chemical Engineering* 74, 464–470.
- [45] Hoffmann, A. C., Stein, L. E., 2008. *Gas cyclones and swirl tubes: Principle, Design and Operation*, 2nd Edition. Springer.
- [46] Holland, J. H., 1975. *Adaptation in Natural and Artificial Systems*. The University of Michigan Press, Ann Arbor.
- [47] Horvath, A., Jordan, C., Harasek, M., 2008. Influence of vortex-finder diameter on axial gas flow in simple cyclone. *Chemical Product and Process Modeling* 3 (1), 1–26.
- [48] Hu, L. Y., Zhou, L. X., Zhang, J., Shi, M. X., March 2005. Studies on strongly swirling flows in the full space of a volute cyclone separator. *AIChE Journal* 51 (3), 740–749.
- [49] Karagoz, I., Avci, A., 2005. Modelling of the pressure drop in tangential inlet cyclone separators. *Aerosol Science and Technology* 39 (9), 857–865.
- [50] Katenka, N., 2013. How to check if the distribution is indeed normal? [http://math.bu.edu/people/nkatenka/MA115\\_FALL2010/QQPlot.pdf](http://math.bu.edu/people/nkatenka/MA115_FALL2010/QQPlot.pdf).
- [51] Kaya, F., Karagoz, I., 2009. Numerical investigation of performance characteristics of a cyclone prolonged with a dipleg. *Chemical Engineering Journal* 151, 39–45.
- [52] Kecman, V., 2001. *Learning and soft computing: support vector machines, neural networks, and fuzzy logic models*. MIT press.
- [53] Kirkpatrick, S., Jr., D. G., Vecchi, M. P., 1983. Optimization by simulated annealing. *science* 220 (4598), 671–680.
- [54] Liu, S., Xu, L., Li, D., Li, Q., Jiang, Y., Tai, H., Zeng, L., 2013. Prediction of dissolved oxygen content in river crab culture based on least squares support vector regression optimized by improved particle swarm optimization. *Computers and Electronics in Agriculture* 95, 82–91.
- [55] Matlab, 2012. *User Guide, Matlab R2012b*. The MathWorks, Inc.
- [56] McKay, M. D., Beckman, R. J., Conover, W. J., 1979. Comparison of three methods for selecting values of input variables in the analysis of output from a computer code. *Technometrics* 21 (2), 239–245.

- [57] Mercer, J., 1909. Functions of positive and negative type, and their connection with the theory of integral equations. *Philosophical transactions of the royal society of London. Series A, containing papers of a mathematical or physical character* 209, 415–446.
- [58] Myers, R. H., Montgomery, D. C., Anderson-Cook, C. M., 2009. *Response Surface Methodology: Process and Product Optimization Using Designed Experiments*, 3rd Edition. Wiley series in probability and statistics. Wiley, Hoboken, N.J.
- [59] Nelder, J. A., Mead, R., 1965. A simplex method for function minimization. *The Computer Journal* 7 (4), 308–313.
- [60] O’Doherty, T., Griffiths, A. J., Syred, N., Bowen, P. J., Fick, W., 1999. Experimental analysis of rotating instabilities in swirling and cyclonic flows. *Developments in Chemical Engineering and Mineral Processing* 7, 245–267.
- [61] Qian, F., Zhang, M., 2005. Study of the natural vortex length of a cyclone term with response surface methodology. *Computers and Chemical Engineering* 29, 2155–2162.
- [62] Ramachandran, G., Leith, D., Dirgo, J., Feldman, H., 1991. Cyclone optimization based on a new empirical model for pressure drop. *Aerosol Science and Technology* 15, 135–148.
- [63] Samui, P., 2011. Application of least square support vector machine (lssvm) for determination of evaporation losses in reservoirs. *Engineering* 3 (4), 431–434.
- [64] Shepherd, C. B., Lapple, C. E., September 1940. Flow pattern and pressure drop in cyclone dust collectors cyclone without intel vane. *Industrial & Engineering Chemistry* 32 (9), 1246–1248.
- [65] Shukla, S. K., Shukla, P., Ghosh, P., 2010. Evaluation of numerical schemes using different simulation methods for the continuous phase modeling of cyclone separators. *Advanced Powder Technology* 22 (2), 209–219.
- [66] Singh, K. P., Basant, N., Gupta, S., Sinha, S., 2011. Support vector machines in water quality management: a case study. *Analytica chimica acta*.
- [67] Slack, M. D., Prasad, R. O., Bakker, A., Boysan, F., 2000. Advances in cyclone modeling using unstructured grids. *Trans IChemE. 78 Part A*, (2000).
- [68] Solero, G., Coghe, A., 2002. Experimental fluid dynamic characterization of a cyclone chamber. *Experimental Thermal and Fluid Science* 27, 87–96.
- [69] Stairmand, C. J., 1949. Pressure drops in cyclone separators. *Industrial and Engineering Chemistry* 16 (B), 409–411.

- [70] Stairmand, C. J., 1951. The design and performance of cyclone separators. *Industrial and Engineering Chemistry* 29, 356–383.
- [71] Suykens, J. A. K., Gestel, T. V., Brabanter, J. D., Moor, B. D., Vandewalle, J., 2002. *Least squares support vector machines*. World Scientific, Singapore.
- [72] Vapnik, V., 1995. *The nature of statistical learning theory*. Springer, New York.
- [73] Vapnik, V., 2000. *The nature of statistical learning theory*, 2nd Edition. Information Science and Statistics. Springer.
- [74] Xiang, R., Park, S. H., Lee, K. W., 2001. Effects of cone dimension on cyclone performance. *Journal of Aerosol Science* 32 (4), 549–561.
- [75] Yazdabadi, P. A., Griffiths, A. J., Syred, N., 1994. Characterization of the PVC phenomena in the exhaust of a cyclone dust separator. *Experiments in Fluids* 17, 84–95.
- [76] Zameer, A., Mirza, S. M., Mirza, N. M., 2014. Core loading pattern optimization of a typical two-loop 300 MWe PWR using simulated annealing (SA), novel crossover genetic algorithms (GA) and hybrid GA(SA) schemes. *Annals of Nuclear Energy* 65 (0), 122 – 131.
- [77] Zhang, B., Hui, S., October 2007. Numerical simulation and PIV study of the turbulent flow in a cyclonic separator. In: *International Conference on Power Engineering*. Hangzhou, China.
- [78] Zhao, B., 2004. A theoretical approach to pressure drop across cyclone separators. *Chemical Engineering Technology* 27, 1105–1108.
- [79] Zhao, B., 2009. Modeling pressure drop coefficient for cyclone separators a support vector machine approach. *Chemical Engineering Science* 64, 4131–4136.
- [80] Zhao, B., Su, Y., 2010. Artificial neural network-based modeling of pressure drop coefficient for cyclone separators. *chemical engineering research and design* 88, 606–613.

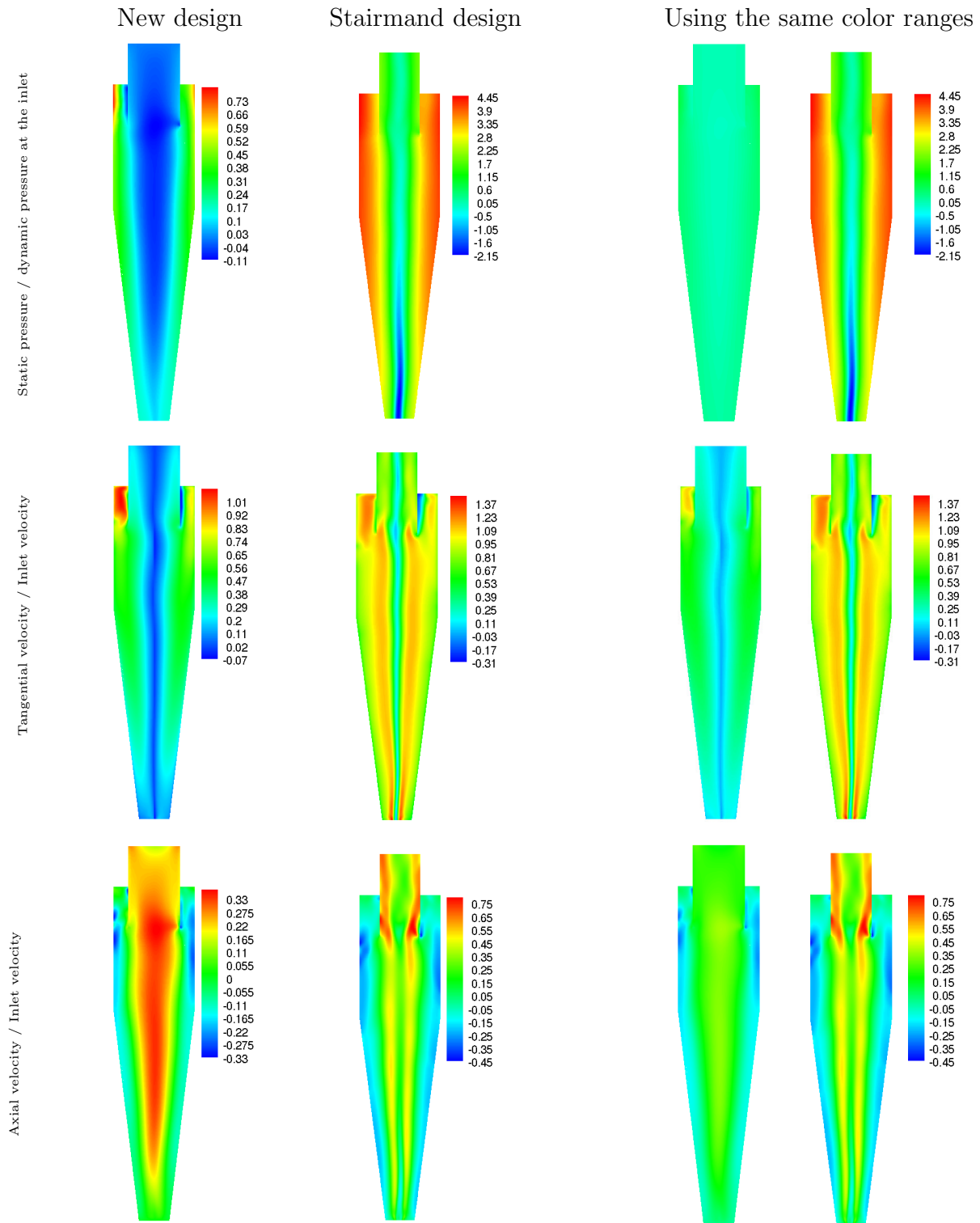


Figure 10: Contour plots for the time averaged dimensionless flow variables throughout the mid plane ( $Y=0$ )

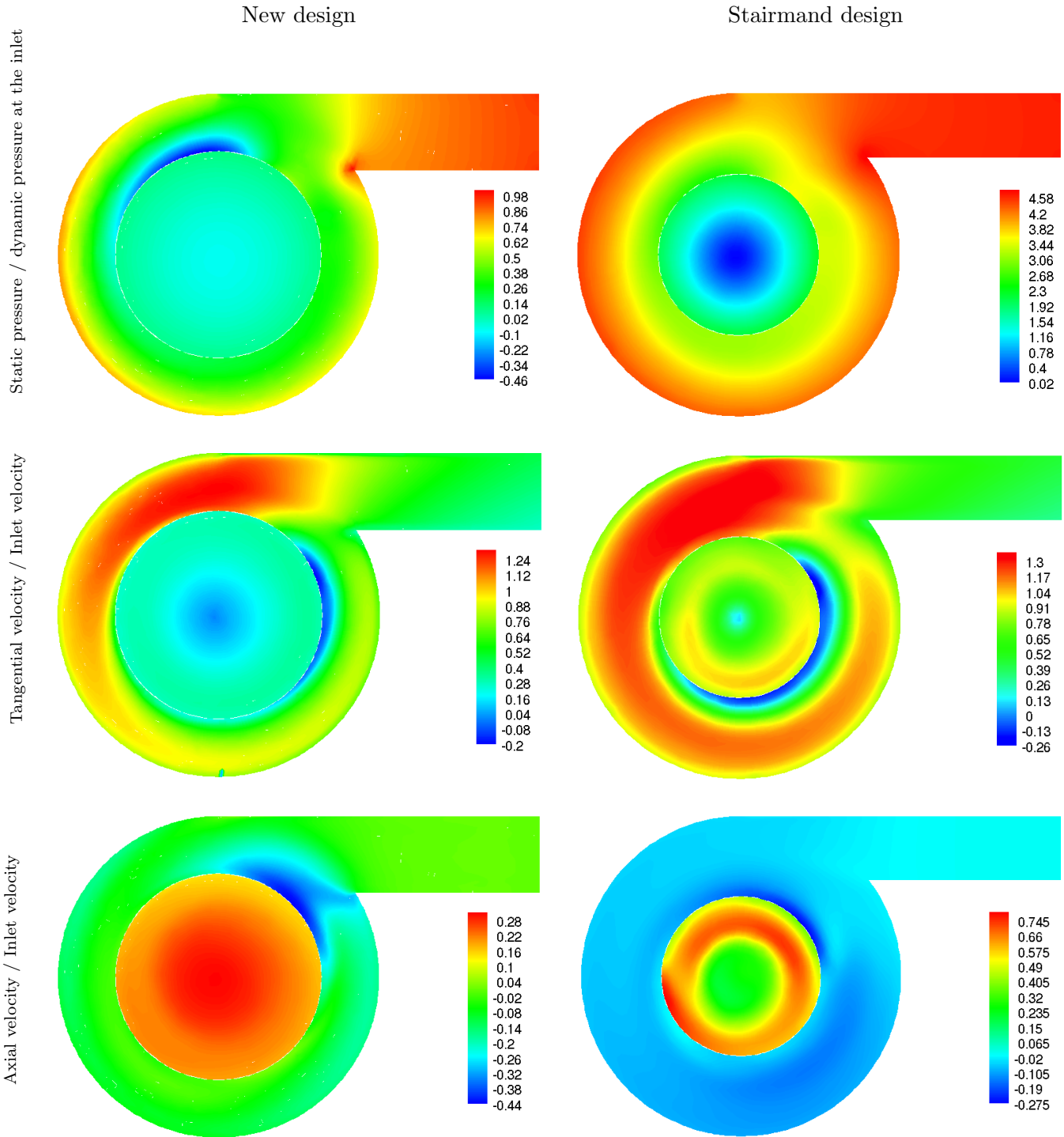


Figure 11: Contour plots of the time averaged dimensionless flow variables through the inlet section



New design

Stairmand design

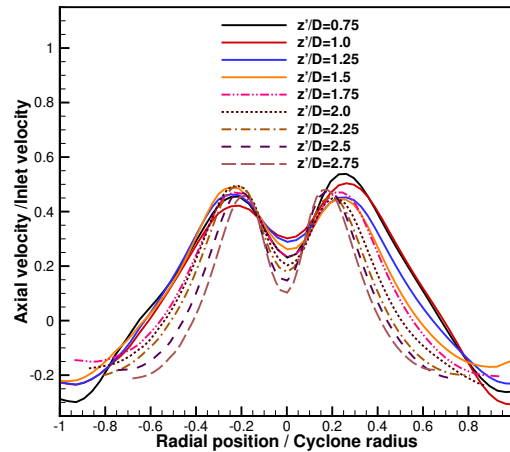
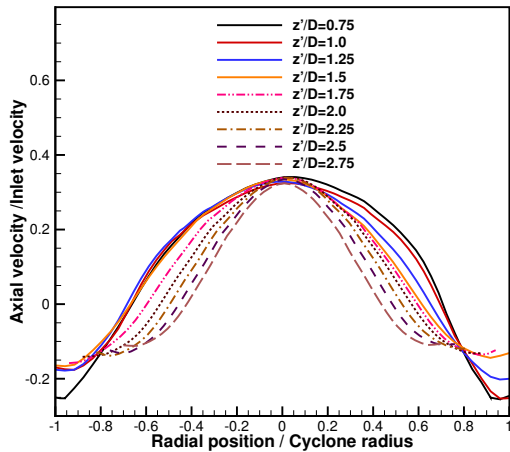
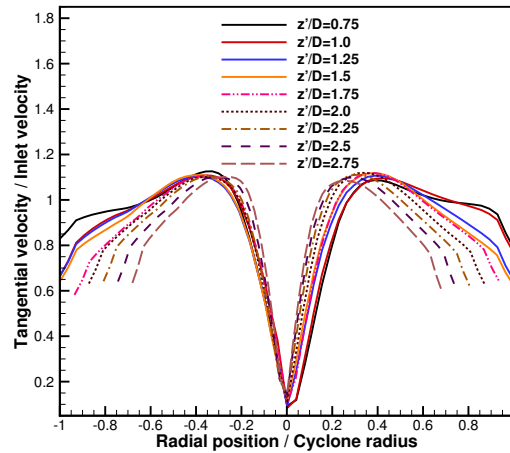
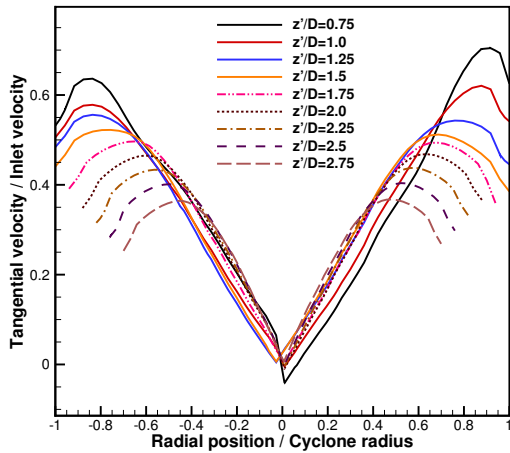
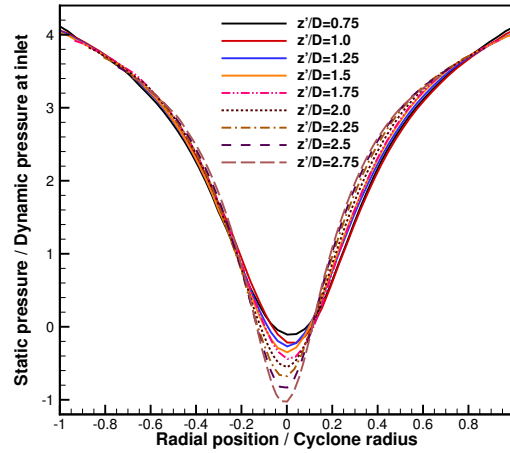
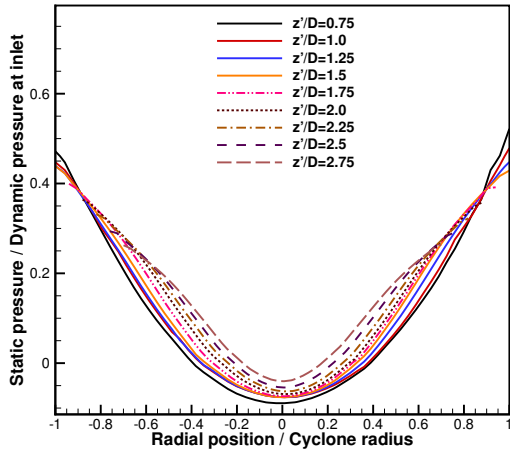


Figure 12: Axial variations of the time averaged dimensionless flow variables

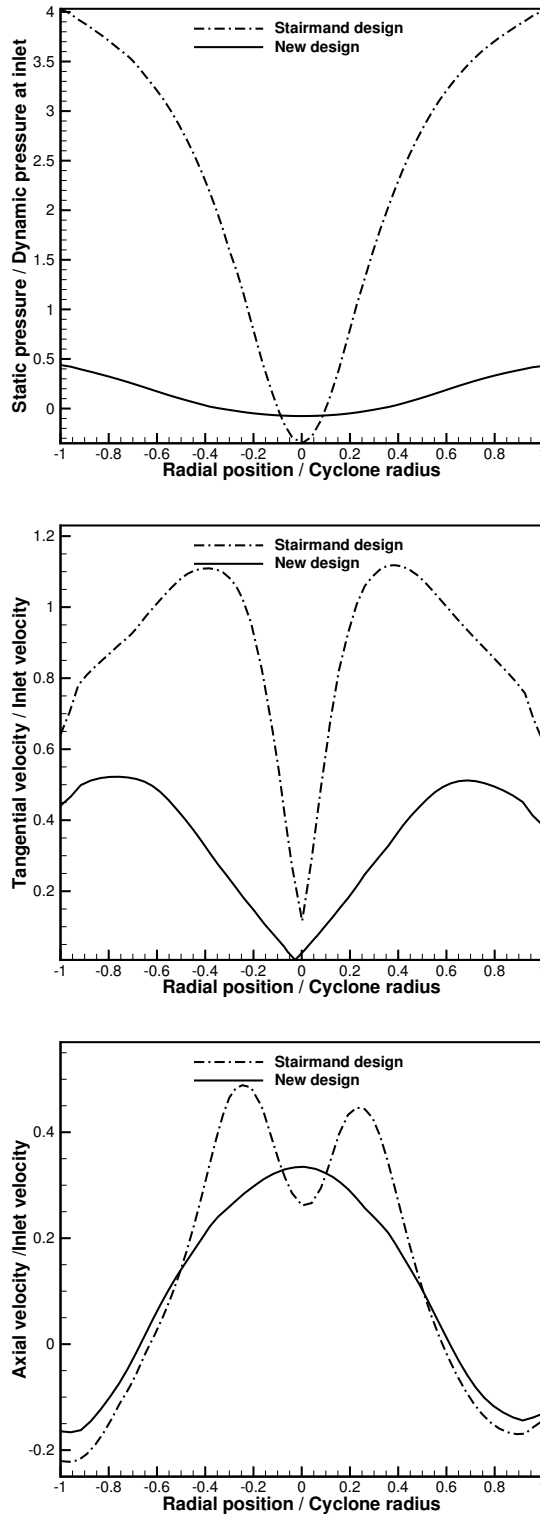


Figure 13: Comparison between the radial profile for the dimensionless flow variables for the two designs at  $z/D = 1.5$